# Early cerebrovascular and long-term neurological modifications ensue following juvenile mild traumatic brain injury in male mice

Aleksandra Ichkova, Beatriz Rodriguez-Grande, Emma Zub, Amel Saudi, Marie-Line Fournier, Justine Aussudre, Pierre Sicard, André Obenaus, Nicola Marchi, Jerome Badaut

# Early cerebrovascular and long-term neurological modifications ensue following juvenile mild traumatic brain injury in male mice

Aleksandra Ichkova[a], Beatriz Rodriguez-Grande[a], Emma Zub[f], Amel Saudi[f], Marie-Line Fournier[a], Justine Aussudre[a], Pierre Sicard[g], André Obenaus[a,b,c,d,e], Nicola Marchi[f,**], Jerome Badaut[a,c,*]

[a] CNRS UMR5287, University of Bordeaux, Bordeaux, France
[b] Department of Pediatrics, Loma Linda University School of Medicine, Loma Linda, CA, USA
[c] Basic Science Department, Loma Linda University School of Medicine, Loma Linda, CA, USA
[d] Center for Glial-Neuronal Interactions, Division of Biomedical Sciences, UC Riverside, Riverside, CA, USA
[e] Department of Pediatrics, University of California, Irvine, Irvine, CA, USA
[f] Cerebrovascular and Glia Research Laboratory, Department of Neuroscience, Institute of Functional Genomics (UMR 5203 CNRS–U1191 INSERM, University of Montpellier), Montpellier, France
[g] INSERM, CNRS, Université de Montpellier, PhyMedExp, IPAM, Montpellier, France

ARTICLE INFO

*Keywords:*
Head trauma
Pediatric
Cerebrovascular oxygenation
Blood-brain barrier
Cerebrovascular damage
Vasoreactivity
Neurological sequel

ABSTRACT

Clinical evidence suggests that a mild traumatic brain injury occurring at a juvenile age (jmTBI) may be sufficient to elicit pathophysiological modifications. However, clinical reports are not adequately integrated with experimental studies examining brain changes occurring post-jmTBI. We monitored the cerebrovascular modifications and assessed the long-term behavioral and electrographic changes resulting from experimental jmTBI.

*In vivo* photoacoustic imaging demonstrated a decrease of cerebrovascular oxygen saturation levels in the impacted area hours post-jmTBI. Three days post-jmTBI oxygenation returned to pre-jmTBI levels, stabilizing at 7 and 30 days after the injury. At the functional level, cortical arterioles displayed no NMDA vasodilation response, while vasoconstriction induced by thromboxane receptor agonist was enhanced at 1 day post-jmTBI. Arterioles showed abnormal NMDA vasodilation at 3 days post-jmTBI, returning to normality at 7 days post injury. Histology showed changes in vessel diameters from 1 to 30 days post-jmTBI. Neurological evaluation indicated signs of anxiety-like behavior up to 30 days post-jmTBI. EEG recordings performed at the cortical site of impact 30 days post-jmTBI did not indicate seizures activity, although it revealed a reduction of gamma waves as compared to age matched sham. Histology showed decrease of neuronal filament staining. In conclusion, experimental jmTBI triggers an early cerebrovascular hypo-oxygenation *in vivo* and faulty vascular reactivity. The exact topographical coherence and the direct casualty between early cerebrovascular changes and the observed long-term neurological modifications remain to be investigated. A potential translational value for cerebro-vascular oxygen monitoring in jmTBI is discussed.

## 1. Introduction

Traumatic brain injury (TBI) is the leading cause of death and disability in the pediatric population. At least 75% of all cases of pediatric TBI (≤18-years-old) in the USA are mild (Lumba-Brown et al., 2018). Mild TBI (mTBI) encompasses no, or transient loss of consciousness and no visible computed tomography (CT)-scan alterations (Barkhoudarian et al., 2016; Petraglia et al., 2014a). Nevertheless, increasing evidence suggests that after mTBI pediatric subjects may develop neurological impairment years after the initial injury, including depression, anxiety, persistent headaches or fatigue, associated or not to post-concussive encephalopathy (Anderson et al., 2012; Babikian et al., 2015; Dean and Sterr, 2013). Currently, diagnosis and prognosis of mTBI in the pediatric population remains inadequate, mostly a reflection of an incomplete understanding of the pathological changes developing over time after the initial impact.

It is now accepted that cerebrovascular dysfunction promotes or sustains abnormal neuronal activity (Giannoni et al., 2018; Klement

* Correspondence to: J. Badaut, Brain Molecular Imaging group, CNRS UMR 5287, Bordeaux University, 146 rue Léo Saignat, 33076 Bordeaux, cedex, France.
** Correspondence to: N. Marchi, Cerebrovascular and Glia Research, Institute of Functional Genomics, (CNRS UMR5203, INSERM U1191, University of Montpellier), 141 rue de la Cardonille, 34094 Montpellier, Cedex 5, France.
*E-mail addresses:* nicola.marchi@igf.cnrs.fr (N. Marchi), jerome.badaut@u-bordeaux.fr (J. Badaut).

et al., 2018; Marchi and Lerner-Natoli, 2013) and accelerating neuronal degenerative processes (Montagne et al., 2017). Disturbance of blood supply and cerebrovascular damage during the pediatric period can have devastating consequences, promoting long-term alterations (Adelson et al., 2011; Philip et al., 2009; Vavilala et al., 2004; Vavilala et al., 2008). Importantly, moderate and severe pediatric TBI are associated with edema formation and dysregulation of cerebral blood flow (CBF), frequently observed along with behavioral deficits (Ichkova et al., 2017; Pop and Badaut, 2011). Cerebrovascular dysfunction after moderate and severe pediatric TBI is a proposed predictor of poor long-term outcome (Philip et al., 2009). Whether similar events and mechanisms apply to pediatric mTBI remains unclear.

Here, we asked whether mTBI delivered on post-natal day 17 mice (Rodriguez-Grande et al., 2018) elicits an early cerebrovascular dysfunction. We examined the pattern of cerebrovascular oxygenation in vivo, vascular reactivity, blood-vessel morphology, behavioral outcome and late-stage neurophysiological modifications by electrographic recording in four sets of experiments (Fig. 1A). Our experimental design did not allow resolving the direct causality or association between early and long-term events.

## 2. Materials and methods

### 2.1. Animals

All experiments were conducted in strict compliance with the European Directive (2010/63/EU) and the French law governing the use of laboratory animals and were approved by local Ethic Committees (authorization#11435–2,017,090,814,307,570.v3;#19102–2,019,062,514,062,187.v2). Animal reporting was performed according to ARRIVE guidelines.

C57BL/6 breeder mice were supplied by Janvier Labs (France) and mouse pups were bred in-house. Cages contained standard bedding and enrichment material. Animals were maintained at 21 °C ± 1 °C, 55% ± 10% humidity, in a 12h–12 h light–dark cycle and had ad libitum access to food and water at all times. Closed head injury was performed on postnatal day (pnd) 17 male pups as described below. In this exploratory work we decided to focus on male pups. Mice over 6 g at pnd17 were used. Juvenile mice ($n$ = 164 mice) were weighed and randomly assigned (6.9 ± 0.1, $n$ = 66 for sham group and 6.9 ± 0.1, $n$ = 71 for jmTBI group) to four independent experimental groups (Fig. 1A). The number of animals used in each outcome measure and the respective time-points after injury are shown in supplementary Table 1 and the flowchart (Fig. 1A). Evaluations were blinded for the experimental groups: photoacoustic imaging (PS), MRI (AO), histology regional analysis (AI), vascular reactivity (AI), vessels diameter analysis (AI), Western blot (AI), behavior (BRG), EEG (EZ).

### 2.2. Juvenile mild traumatic brain injury (jmTBI) model: closed-head injury with long-term disorders (CHILD)

Closed head injury in pnd17 mouse pups using the CHILD model was performed as previously described (Rodriguez-Grande et al., 2018). Briefly, mice were anesthetized using 2.5% isoflurane and 1.5 L/min air for 5 min and then placed under the electromagnetic impactor (Leica Impact One Stereotaxic impactor, Leica Biosystems, Richmond, IL, USA) over an aluminum foil surface. To incorporate both focal damage and head rotation in a closed head injury model in juvenile mice, the head was not restrained. To avoid surgical artifacts, we did not perform a craniotomy, nor a skin incision. The impact was made over the intact mouse head, and thus a light anesthesia sufficed. The injury was produced with a 3 mm round tip at a speed of 3 m/s, with a depth of 3 mm and a dwell time of 0.1 s. The tip of the impactor was located over the left somatosensory and parietal cortex center at approximately Bregma −1.7 mm, and approximately −1.5 mm from the midline. Sham mice were anesthetized and placed under the impactor, but did not receive any impact. After the impact mice were left to recover in an empty cage. There is no mortality in this jmTBI model. After injury, jmTBI mice exhibited a longer time to stand (median of Sham = 135.0 s, $n$ = 65 vs median of jmTBI = 411 s, $n$ = 67, $p$ < .0001, Mann Whitney test) and to explore than the sham group (median of Sham = 392 s, n = 65 vs median of jmTBI = 791 s, n = 67, p < .0001, Mann Whitney test) after recovery from anesthesia (Fig. 1B).

### 2.3. Photoacoustic imaging of cerebrovascular oxygenation

Longitudinal variations in cerebrovascular oxygenation in vivo after jmTBI were evaluated using photoacoustic imaging (PAI). PAI is a hybrid imaging modality that combines optical imaging and ultrasound for fusion of anatomical and functional imaging data. PAI allows to detect the acoustic signals generated by optical absorption from endogenous chromophore such as oxygenated and deoxygenated hemoglobin. Imaging sessions were longitudinal performed on the same mouse at 6 h and at, 3, 7 and 30 days after head impact (sham $n$ = 10; jmTBI n = 10). All imaging was performed using a Vevo LAZR-X imaging system (FUJIFILM VisualSonics, Inc., Toronto, ON, Canada). During the 3–4 min imaging sessions, mice were anesthetized using 1.5% isoflurane mixed with air to immobilize the animals. Mice were placed on heated imaging platform in prone position. Ultrasound gel was applied on top of the head and in the transducer cavity to ensure that no air bubble was present during PAI. Three-dimensional PAI was performed in “oxyhemo” mode to obtain parametric maps of saturated O2 (sO2) and total hemoglobin (Hbt) concentration, scanning from the occipital region to frontal region of the mouse brain. An automated imaging sequence was used to perform dual-wavelength PAI at 750 and 850 nm with 34 dB gain. Arrival time gain compensation was applied to account for photoacoustic signal loss for all imaging sessions. Mouse brain was imaged using an MX250 transducer (FUJIFILM VisualSonics) with a broadband frequency range from 13 to 24 MHz and operating at a center frequency of 20 MHz. Three-dimensional PAI was then performed using the acquisition motor with a scanning range of 1.5 cm and step size of 0.15 mm. A region of interest (ROI) was delineated manually based on the anatomic ultrasound images from the occipital region to frontal region of the mouse brain. Quantitative analysis of oxy-hemo PAI was performed offline using the VevoLab Software 3.1.1 (FUJIFILM VisualSonics).

### 2.4. Telemetry video-electrocorticography

Three to four weeks post-jmTBI mice (sham $n$ = 3; jmTBI $n$ = 4) were anesthetized using (Ketamine 100 mg/kg + Xylazine 10 mg/kg) and surgery performed to implant two micro screw in the skull (bipolar electrode) around the impacted cortical brain region (Bregma x = 0 and 3 mm; y = −1,7). Screws were wired-connected to a DSI telemetry transmitter (DSI implant TA11ETA-F10). Technically, surgery was feasible and without complications at the chosen mouse age (PND 40–45), ensuring a robust monitoring over time. The transmitter was positioned under the skin on the back of the mouse. Immediately after surgery all mice received intraperitoneal injections of 4% glucose and metoxasol in water. Animals were then allowed to recover from surgery for 5–7 days. Each mouse was recorded (sampling rate 500 Hz, unfiltered) for a total of 24 h and all mice were monitored over a period of 7 days. Data were acquired using Ponemah Software (DSI matrix 2.0; v5.32 Video). Sham and TBI animals were recorded following an identical and precise day/night time schedule, taking into account: (i) light vs. dark phases; (ii) awake/exploratory vs. sleep. Seizure analysis was performed as follow (Girard et al., 2019; Zub et al., 2019): 1) setting a threshold for spike detection of 2.5 × times the standard deviation of the baseline; 2) minimum and maximum spike duration (1 and 100 ms); 3) minimum train-spike duration 5 s with a minimum numbers of spikes of 5 (at least 1 Hz). Minimum separation between two seizures: 1 s. Peak detection was visually re-checked a posteriori.

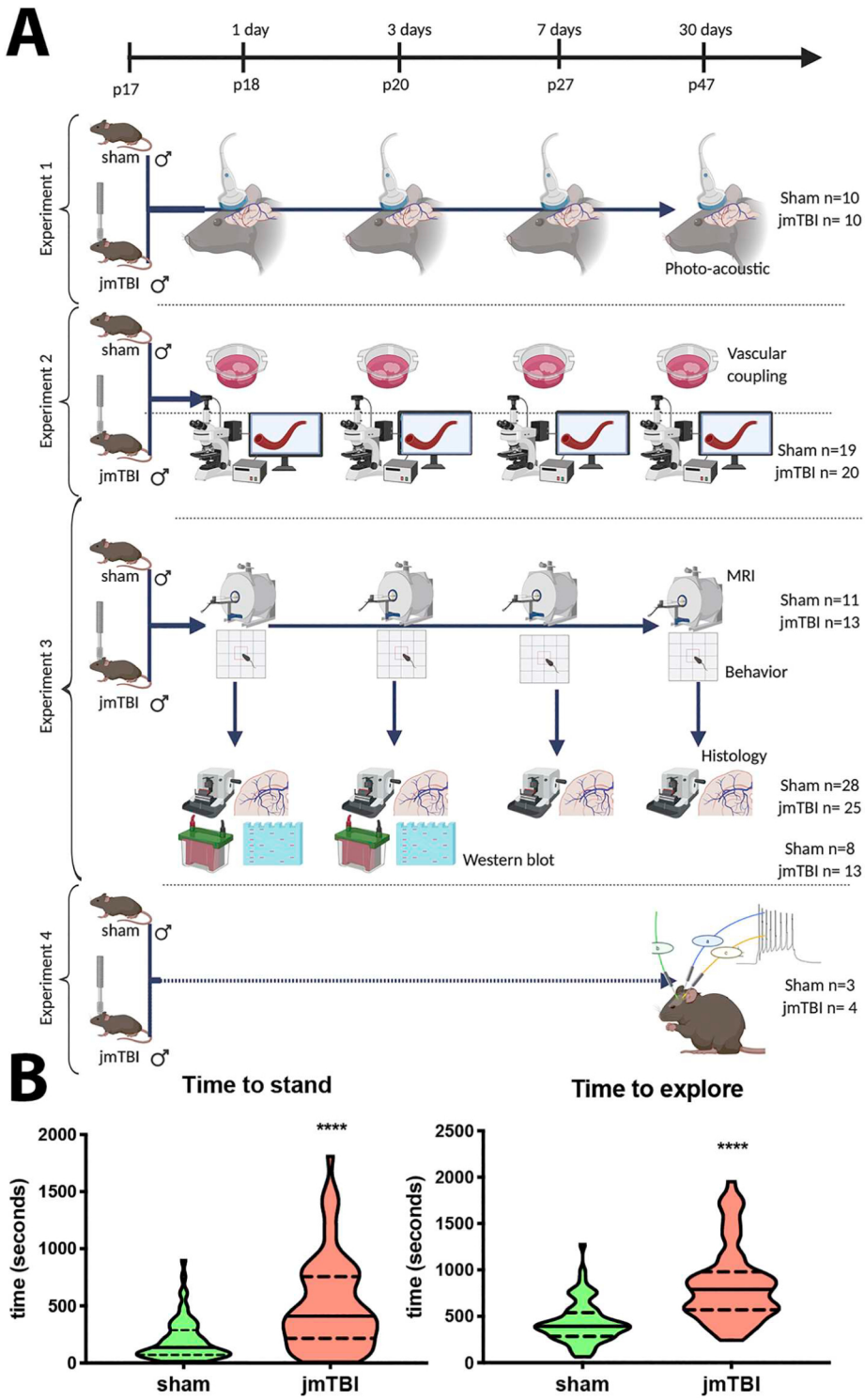


**Fig. 1.** Experimental design and time to recover from anesthesia.
**A** Schematic drawing of the experimental design with 4 independent experiments. **B** The time to stand (median of Sham = 135.0 s, $n$ = 65 vs median of jmTBI = 411 s, $n$ = 67, $p < .0001$, Mann Whitney test) and to explore (median of Sham = 392 s, n = 65 vs median of jmTBI = 791 s, n = 67, p < .0001, Mann Whitney test) after anesthesia were longer for the jmTBI compared to sham group.

Next, EEG portions were selected from each recording (for a total duration of 30 min for each mouse). Results in Fig. 5B refer to the analysis of EEG portions corresponding to immobility states as assessed by video (no walking, no drinking, eating, or scratching) and motion detection as provided by the telemetry transmitter/plaque, during night (dark) periods (10 pm to 5 am) for all sham and all post-jmTBI mice. Using Neuroscore v3.2.0, mouse-specific periodograms Power Bands (binned as 0.5-Hz increment; from 0.5 to 90 Hz) were automatically calculated for each EEG (data output is provided as percentage abundance). Origin microcal was used to plot X/Y graphs, indicating percentage signal (0–100%) on the Y-axis and the continuous frequency interval (0–90 Hz) on the X-axis, as previously reported (Boussadia et al., 2016; Boussadia et al., 2018). Percentage for the gamma wave interval was calculated using Neuroscore.

### 2.5. Open field assay

The open field test was performed around 9:00 am as previously described (Rodriguez-Grande et al., 2018). Briefly, a given mouse was placed in the center of the open field (i.e., a square chamber of 45 × 45cm perimeter and 35 cm height, p) and recorded for 5 min with a camera (Fujiform, Imaging Source, Germany) placed above the chamber. Open field arena was cleaned with a 50% EtOH solution after each use. ANY-maze software (Stoelting Co., Italy) was used to define a central area of 35 × 35cm in the center of the open field chamber. Mouse movement was tracked using ANY-maze, providing parameters that reflect general motor activity and anxiety-like behavior (i.e. mean speed, total distance and percentage of time is spent in the center) for sham ($n$ = 11) and jmTBI ($n$ = 13) at 1, 3, 7, 30dpi (Fig. 1A) (Rodriguez-Grande et al., 2018). No baseline OF test was done in the pups because separation from the mother in pups is highly anxiogenic (Rodriguez-Grande et al., 2018).

### 2.6. Magnetic resonance imaging (MRI) and analysis

In vivo MRI was performed as previously described (Rodriguez-Grande et al., 2018). Briefly, MRI was performed at 1, 3, 7 and 30 days post-injury (dpi) (sham n = 11; jmTBI n = 13) in a 4.7 T scanner (Bruker BioSpin, city state) (1 to 7dpi) and a 7 T scanner (Bruker BioSpin) (for 30dpi) under isoflurane anesthesia (3% for induction and 2% for maintenance in 1.5 l/min of synthetic air). Parametric maps for T2 were processed using Jim Software (Xinapse, England). REgions Region of interests (ROIs) in the ipsilateral cortex were outlined on T2WI and then pasted onto parametric maps using Cheshire software (Hayden Image/Processing Group, Waltham, MA, USA).

### 2.7. Immunohistochemistry and image analysis

For immunohistochemistry investigations, animals were transcardially perfused (1, 3, 7, 30 dpi) with 4% paraformaldehyde, brains were extracted and post-fixed 24 h in the same fixative solution (sham $n$ = 28; jmTBI $n$ = 25). Coronal sections were cut at 50 µm thickness using a vibratome (Leica, Richmond, IL) and stored at −20 °C in cryoprotective medium (30% ethylene glycol and 20% glycerol in phosphate-buffered saline (PBS)) until immunohistochemical analysis (Badaut et al., 2011; Rodriguez-Grande et al., 2018).

Primary antibodies used: rabbit polyclonal against Neuronal Nuclei (NeuN, 1:500, Abcam, Cambridge, MA), Neurofilament 200 (NF200, 1:500, Chemicon International, Temecula, CA, USA), Myelin Basic Protein (MBP, 1:300, Wako, Richmond, VA), rabbit monoclonal amyloid precursor protein (APP) antibody [Y188] (1:500, Abcam, Cambridge, MA) and rabbit polyclonal antibody for smooth muscle actin (SMA, 1:300, Abcam, Cambridge, MA). The secondary antibodies were: IRDye 680 donkey anti-rabbit (Molecular Probes, Invitrogen), IRDye 800 conjugated affinity purified donkey anti-mouse IgG (1:1000, Rockland, Gilbertsville, PA) for NeuN and IgG extravasation, and Alexa-Fluor-594 nm goat anti-rabbit and Alexa 488 nm conjugated affinity purified goat anti-rabbit IgG (1:1000, Invitrogen, Carlsbad, CA) for NF200, APP and MBP. Labeling of the vessels was performed using tomato lectin (1:200, Vector Laboratories, Burlingame, CA).

Free-floating sections were washed with PBS and then placed in a blocking solution (1% bovin serum albumin, BSA and 0,3% Triton X-100 in PBS) for 1 h at room temperature (RT), followed by overnight incubation at 4 °C with the primary antibodies diluted in the same blocking solution. The next day slices were washed in PBS, incubated with the secondary fluorescent antibodies in blocking solution for 2 h at RT, and washed in PBS. After washing sections were mounted and kept at 4 °C until the time of analysis.

For image acquisition of infrared-labeled sections, slides were scanned using an Odyssey infrared scanner (Licor Bio-science, Lincoln, NE, USA) at 21 µm/pixel resolution. Anti-fading medium VectaShield (Vector, Vector laboratories, Burlingame, CA, USA) or Fluoroshield (Sigma-Aldrich, St. Louis, MO) were used and images acquired at 40× (Olympus FV5, Japan) and at 63× magnification (Leica SP8, Leica Microsystems, Germany) .

Image analysis was performed using Fiji software (NIH, USA). ROIs in the ipsilateral cortex for histology matched those used in MRI analysis. ROIs were delineated manually. Blood vessel diameters were measured from the tomato lectin images obtained on confocal microscope with 1 um step size for the z-stack. We obtained 2 z stacks per ipsilateral cortex from 2 cortical levels around the injury site (Bregma 1.2 – Bregma 2.2), in total 4 images per animal. A total of 305 ± 68 blood vessel diameters was measured manually (done by A.I.). The intensity of the immunostaining was quantified in arbitrary units (A.U.) from the original pictures using Fiji software (NIH, USA).

To attain immunoglobulin G (IgG) and tomato lectin staining, sections were washed with PBS, blocked with 1% BSA and 0,3% Triton X-100 in PBS, then incubated for 2 h at room temperature with IRDye 800 conjugated affinity purified goat anti-mouse IgG (1:1000, Rockland, Gilbertsville, PA) or tomato lectin (1:200, Vector Laboratories, Burlingame, CA) in the same blocking solution. After washing, sections were scanned on an IR scanner (Odyssey) to quantify fluorescence for IgG extravasation.

### 2.8. Vascular reactivity in acute brain slices

Mice (sham $n$ = 12 between 1 and 7dpi; $n$ = 7 for 30dpi; jmTBI $n$ = 5 at 1dpi; $n$ = 6 at 3dpi; n = 5 at 7dpi; $n$ = 4 at 30dpi) were anesthetized with 4% isoflurane, until loss of the tail-pinch reflex. After decapitation, coronal brain slices (250 µm) were cut with vibratome in an ice-cold sucrose-based saline solution containing the following: 2 mM KCl, 0.5 mM $CaCl_2$, 7 mM $MgCl_2$, 1.15 mM $NaH_2PO_4$, 26 mM $NaHCO_3$, 11 mM glucose and 205 mM sucrose. The sucrose-based solution was bubbled with a carbogene mixture of 95% O2 and 5% CO2. Slices were allowed to recover in oxygenated artificial cerebrospinal fluid (aCSF, 130 mM NaCl, 3 mM KCl, 2.5 mM $CaCl_2$, 1.3 mM $MgSO_4$, 0.58 mM $NaH_2PO_4$, 25 mM $NaHCO_3$, 10 mM glucose) for at least 1 h at RT.

Blood vessels were visualized with an upright microscope equipped with differential interference contrast (DIC) and a CCD camera (Hamamatsu, Japan). Parenchymal arterioles were selected in cortical layers I-III of the ipsilateral impacted cortex based on morphology and approximate diameter (10–20 µm)(Zonta et al., 2003). Images were acquired every 15 s with a 40× objective and stored for offline analysis. To determine the baseline arteriole's diameter, video recording of 5 min prior to any drug application was performed. Only arterioles with stable diameter and vessel segments visible in the field of view were chosen for drug application. To induce arteriolar vasoconstriction, U46619, a thromboxane A2 analog (Enzo Life Sciences, Plymouth Meeting, PA) was bath applied at a final concentration of 150 nM, as previously showed to induce 30% decrease in vessels diameter (Blanco et al., 2008). To induce vasodilation of the vessels in response to neuronal activity NMDA (Sigma-Aldrich, St. Louis, MO) was bath applied at final concentration of 100 µM (Rancillac et al., 2006). Analyses of the changes in vascular diameter were performed offline using Fiji software (NIH, USA). Vascular diameter was measured manually at 3 points along the vascular segment in each of the 3 consecutive image frames and then the measurements were averaged. The changes in the vessel diameter were calculated as:

% changes in vascular diameter = ((y2-y1)/y1)*100, where y1 is the baseline diameter and y2 is the diameter after U46619 or NMDA applications.

### 2.9. Western blot

Cortical tissue from sham ($n$ = 8) and jmTBI ($n$ = 13) at 1 and and3 dpi was collected and frozen for Western blot analysis (Badaut et al.,

2011; Jullienne et al., 2018a). Tissue samples were sonicated for 30 s in a tube with RIPA buffer with protease inhibitor cocktail (PIC, Roche) after which the samples were stored at −20 °C. Total protein concentration was measured with the bicinchoninic acid assay (BCA, Pierce Biotechnology Inc., Rockford, IL, USA). Twenty micrograms of protein were then subjected to SDS polyacrylamide gel electrophoresis on a 10% bis-acrylamide gel. Proteins were then transferred to a polyvinylidene fluoride membrane (PerkinElmer, Germany). After the protein transfer, the blot was blocked with Odyssey blocking buffer (LI-COR, Bioscience, Germany) for 1 h at RT and incubated with a mouse monoclonal antibody against SMA (Sigma-Aldrich, St. Louis, MO) and a polyclonal rabbit antibody against tubulin (1:1000, LI-COR Biosciences, Lincoln, NE, USA), or with a rabbit polyclonal antibody against thromboxane A2 receptor (TXA2R, 1:500, Santa Cruz Biotechnology, Dallas, TX) and a mouse monoclonal antibody against actin (1:5000, LI-COR Biosciences, Lincoln, NE, USA) in the same blocking buffer at 4 °C overnight. After washing in PBS for 3x10min, the blot was then incubated with two fluorescence-coupled secondary antibodies (1:10,000, anti-rabbit Alexa-Fluor-680 nm, Molecular Probes, Oregon and anti-mouse infra-red-Dye-800 nm, Roche, Germany) for 2 h at RT. After washing in PBS, the degree of fluorescence was measured using an infrared scanner (Odyssey, LI-COR Biosciences, Lincoln, NE, USA) as previously published (Badaut et al., 2011; Jullienne et al., 2018a). The fluorescence value of the SMA and TXA2R bands was normalized to the tubulin\actin protein bands and compared between the sham and jmTBI group at each time point.

### 2.10. Statistical analysis

Data were analyzed with GraphPad Prism 3.05 (GraphPad Software Inc., USA) using an unpaired *t*-test for the T2WI analysis; one-way or two-way ANOVA's followed by Sidak's and Tukey post-hoc test were used for multiple groups across different time points for photoacoustic imaging, neurovascular coupling and open-field outcomes. Non-parametric Mann Whitney tests were used for time to stand and explore behavioral tests and also for immunostaining measurements. All data are presented as mean ± standard deviation (SD). Significance was set at $p < .05$.

## 3. Results

### 3.1. Immediate cerebrovascular hypoxia and T2WI increase post jmTBI

Longitudinal photoacoustic imaging (PAI) (Fig. 2A) revealed a significant decrease in cerebrovascular oxygen saturation in the impacted left cortex of jmTBI mice at 6 h post injury (Fig. 2B) as compared to age-matched sham animals (50.4 ± 3.9% vs 63.6 ± 1.6% $p < .001$ two-way RM ANOVA, Fig. 2C) and to contralateral hemisphere (example in Fig. 2B). The impacted left hemisphere was the most affected. However, in certain cases the contralateral right hemisphere also presented with transient hypo-oxygenation (data not shown). Oxygen saturation returned to levels comparable to sham animals at 3, 7 and 30 days post-injury (dpi) (Fig. 2C). T2WI did not show major anatomical changes after jmTBI (Fig. 2D), indicating mild severity for the trauma. T2 values were increased at 1dpi (71,68 ± 0,43 ms) in the ipsilateral cortex of jmTBI mice as compared to shams (69,27 ± 0,69 ms, $p < .05$, t-test, Fig. 2E). As observed for cerebrovascular oxygen saturation, ipsilateral cortical T2 values returned to baseline levels at 3, 7 and 30 dpi (Fig. 2E).

### 3.2. Cortical blood vessels reactivity is modified early post-jmTBI

By using an established acute cortical brain slice protocol, we examined the changes of vessel diameter resulting from NMDA application (Blanco et al., 2008; Zonta et al., 2003). We report patterns of vasoreactivity dissimilar between jmTBI and sham slice preparations at 1 and 3 dpi (Fig. 3). The thromboxane A2 agonist U46619 was used to restore vascular tone ex vivo before the application of NMDA (Fig. 3A, B). The vasoconstriction was rapid for blood vessels in slices from 1dpi jmTBI mice compared to blood vessels in sham brain slices (Fig. 3A, C). Arterioles in cortical slices from 3 dpi jmTBI exhibited slower vasoconstriction as compared to sham and 1 dpi jmTBI after U46619 application (Fig. 3C). By 7 dpi, there was no difference of vasoreactivity between sham and jmTBI after the application of U46619 (Fig. 3C, Supplementary Fig. 3). NMDA application on U46619-pre-constricted blood-vessels induced vasodilation in slices obtained from sham and jmTBI 3 dpi (+4.32% ± 9.14 for sham and + 30.13% ± 3.31 for 3 dpi jmTBI, $p < .05$, Fig. 3B, D). An opposite response was observed for blood vessels in slices obtained from jmTBI 1 dpi after NMDA application (vasoconstriction, − 6.60% ± 7.49%; Fig. 3B, D). Taken together, these results indicate modified cortical cerebrovascular reactivity occurring early post-jmTBI.

### 3.3. Histological evaluation of cerebrovascular damage post jmTBI

A significant increase of parenchyma IgG occurred at 1 dpi (430.3 A.U. ± 161.4 vs 100.0 A.U. ± 9.0 in sham, $p < .05$, Mann Whitney test, Fig. 4A, B) in the cortex of jmTBI mice. IgG extravasation was present at the hippocampal level at 1 dpi (Fig. 4A) indicative of diffuse cerebrovascular injury in this model. Starting from 7 dpi IgG extravasation decreased indicating reversible alteration (Fig. 4B), converging with the T2 value read-out (Fig. 2E).

Tomato-lectin positive cortical vessels displayed biphasic morphological changes: 1) at 1 dpi, a ~ 15.5% decrease of diameter size in jmTBI as compared to sham ($p < .0001$,Mann Whitney test, Fig 4C1, C2, D); 2) at 7 dpi, a 12% diameter increase ($p < .01$, Mann Whitney test, Fig 4C3, C4, E), lingering at 30dpi ($p < .01$, Mann Whitney test, Fig 4C5, C6, F) in jmTBI mice. At 3 dpi, vessel diameters were comparable between jmTBI and age-matched sham mice. Diameter distribution analysis is provided in Fig. 4G, showing the increased portion of larger blood vessels with a diameter > 10 µm in jmTBI from 7 to 30 dpi as compared to age-matched sham.

### 3.4. Signs of long-term neurological deficits after jmTBI

We next investigated whether signs of long-term neurological modifications exist after jmTBI. jmTBI Injuried mice spent significantly less time in the center of the open field, suggestive of anxiety-like traits (Fig. 5A). In a separate and limited cohort, we performed a cortical electrographic monitoring at the site of impact, comparing sham to jmTBI animals. Data were obtained starting from 30 dpi, consistently with the earliest mouse age when electrode implant can be adequately performed. Analysis of the entire recordings did not indicate the presence of seizures, repetitive spikes or epileptiform activity under these specific experimental conditions. Interestingly, cortical electrographic recording revealed dissimilar patterns of wave frequency distributions between sham and jmTBI mice (Fig. 5B, C). Specifically, gamma wave relative abundance was decreased in all of the jmTBI mice analyzed as compared to age-matched sham. These initial results are consistent with available reports indicating gamma waves monitoring as a potential biomarker for neurological pathophysiology (Iaccarino et al., 2016; Kitchigina, 2018; Mably and Colgin, 2018). A comprehensive study is required to fully define the dynamics of corticographic modifications over time and as a function of earlier read-outs (e.g., photoacoustic) in the same animal.

### 3.5. Histological evaluation of neuronal damage post-jmTBI

NeuN, NF200 (Fig. 6A, C), MBP (Supplementary Fig. 1A,B) and amyloid precursor protein (APP) immunostainings were performed from 1 to 30 dpi NeuN staining did not reveal significant neuronal loss post-jmTBI in ipsilateral cortex (Fig. 6B, $p > .05$). MBP staining showed

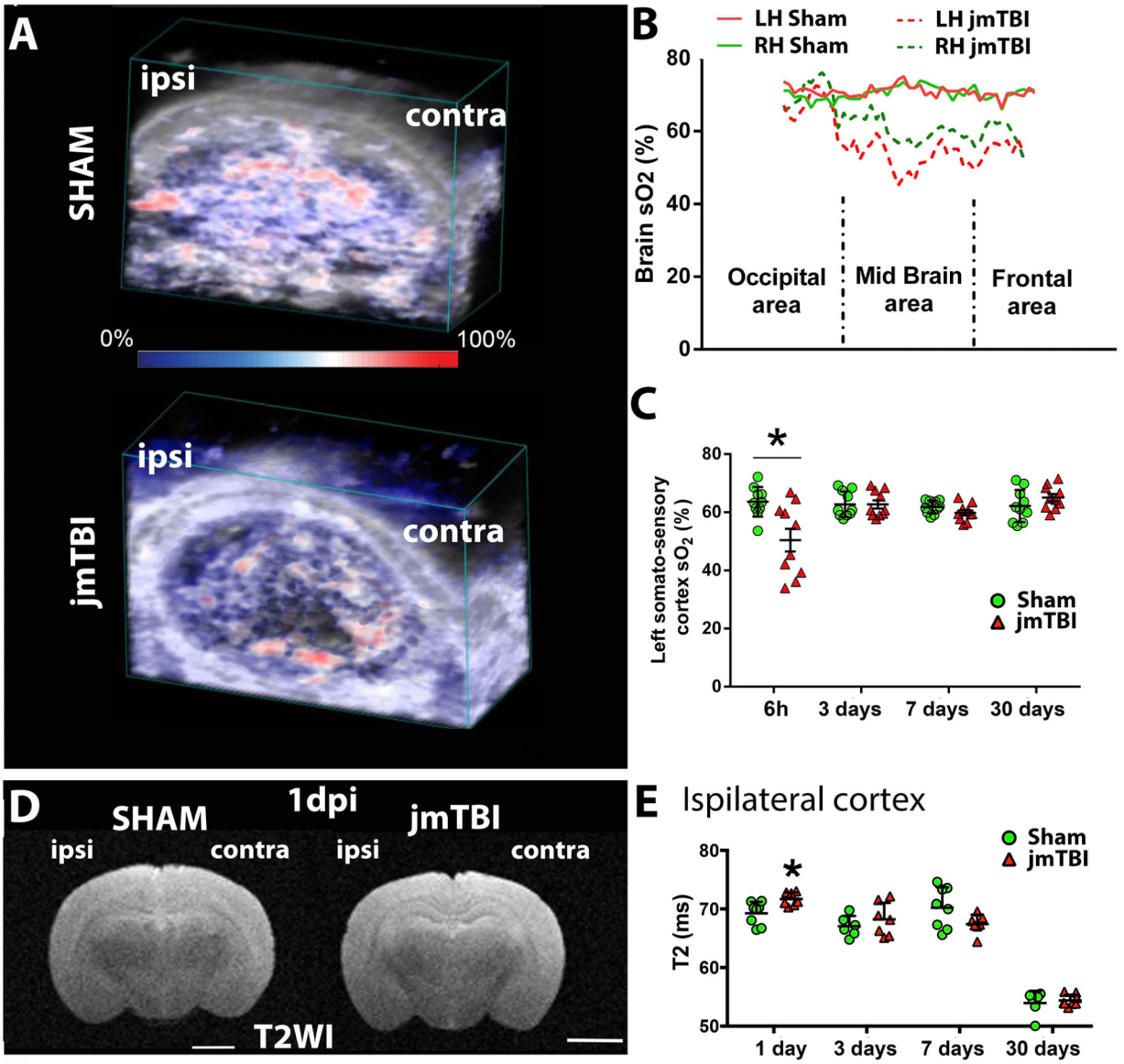


**Fig. 2.** jmTBI induces early transitory cerebrovascular hypoxia and brain edema.
**A:** Representative oxy-hemo photoacoustic images of a sham (top) or jmTBI (bottom) mouse brain presented in 3D. The heat map represents blood oxygen saturation levels ranging from 0% (dark blue) to 100% (dark red). **B**: Representative 6 hours post-injury oxy-hemo photacoustic analyses at the left and right hemisphere of sham and jmTBI mice (frame #20 occipital area, frame #40 mid brain, frame #60 frontal area, left hemisphere, LH; right hemisphere, RH). **C**: Quantification of the oxy-hemo signal in the impacted brain hemisphere (left) showed significant decreased in jmTBI mice at 6 hours post-injury (*$p < .05$, *t*-test) and no changes compared to sham at 3, 7 and 30 dpi ($p > .05$), $n = 10$ animals per group. Contralateral data are not shown. **D**: jmTBI did not result in visible structural changes in the brain (T2 weighted images of sham vs jmTBI at 1 dpi, *scale bar 1.5 mm)***E.** Quantification of the T2 relaxation (ms) in the ipsilateral cortex showed significant increases in jmTBI mice at 1 dpi compared to shams (*p < .05, t-test) but no changes at 3, 7 and 30 dpi (p > .05), n = 6–8 animals per group. (For interpretation of the references to colour in this figure legend, the reader is referred to the web version of this article.)

no significant myelin changes post-jmTBI (Supplementary Fig. 1A, B). APP staining was identical in the cortex for both groups, while APP axonal beading was observed in the corpus callosum of jmTBI mice at 1 dpi (Supplementary Fig. 2). NF200 signal was significantly decreased in the ipsilateral cortex of jmTBI mice as compared to sham at 30 dpi (87.58 ± 2.27 A.U. vs 100.00 ± 3.60 A.U., Mann Whitney test $p < .05$, Fig. 6C, D). These data are suggestive of a delayed axonal pathology in the ipsilateral cortex after jmTBI, although without an overt loss of neurons.

## 4. Discussion

We report sub-cortical cerebrovascular dysfunction(s) rapidly occurring after experimental jmTBI. We also report long-term signs of neurological modifications post-jmTBI. At the impacted somatosensory cortex, the early cerebrovascular changes consisted of: i) cerebrovascular hypoxia in vivo and transient abnormal cerebrovascular reactivity to thromboxane A2 agonist and NMDA ex vivo; ii) transient T2-MRI hyper-intensity suggestive of water accumulation; iii) reduced vessels' diameter as histologically detected early post-jmTBI. At long-term we found: i) increased cortical-vessel diameter; ii) decrease of neurofilament staining with no overt neuronal loss; iii) decreased electrographic gamma waves *in vivo* along with behavioral changes. In the presented study the direct association or causality between early cerebrovascular and late neurological modifications were not examined.

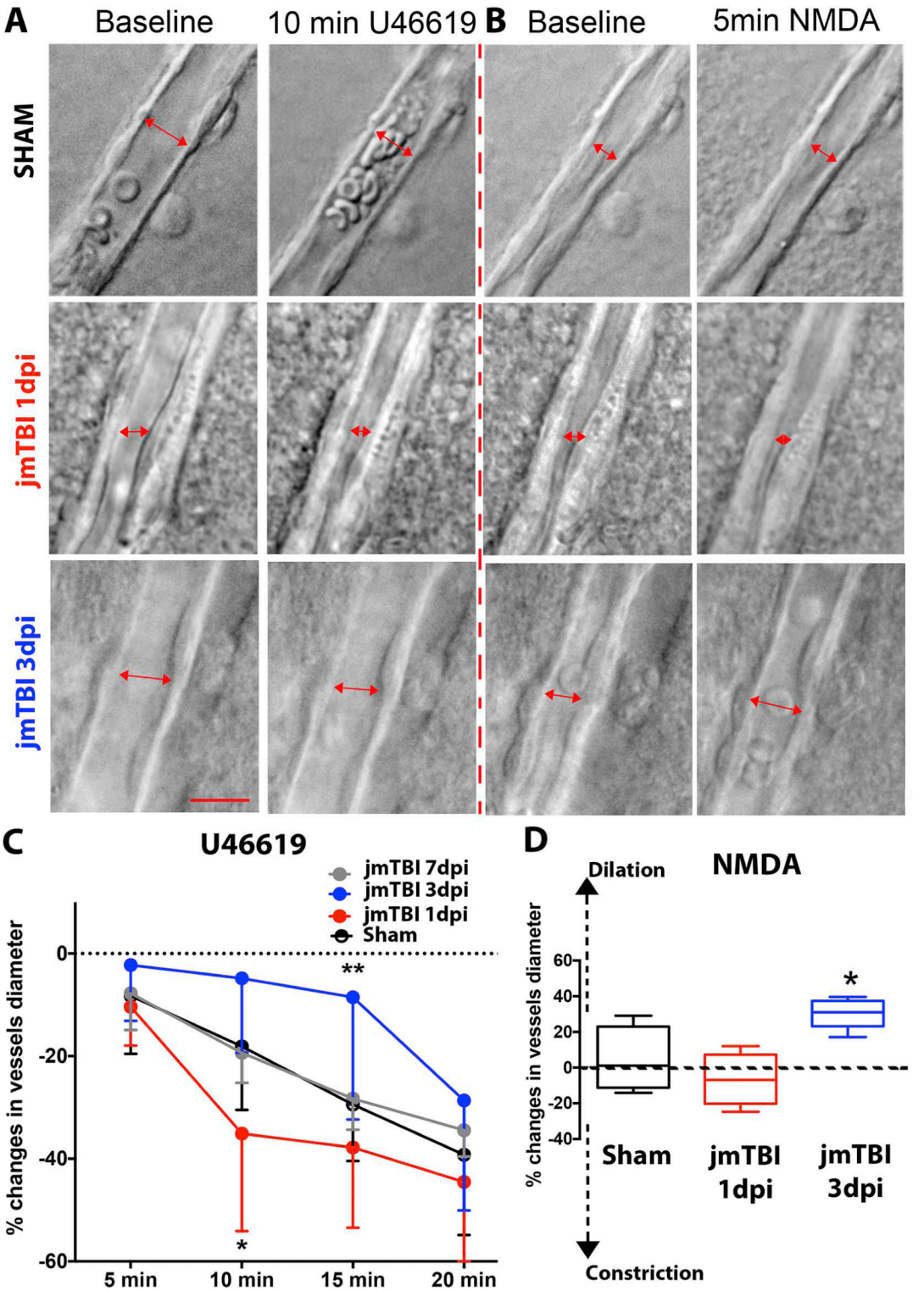


**Fig. 3.** Early and transient modifications of cortical vascular reactivity after jmTBI.
**A.** Examples of cortical blood vessel modifications obtained from sham and jmTBI slices following ten minutes of U46619 application. U46619 induced a decrease of vascular diameter in slices obtained from sham animals. Vasoconstriction of cortical vessel in jmTBI 1 dpi was greater than sham. Vessels in slices obtained from 3 dpi jmTBI mice did not show diameter change after U46619 application. **B.** Application of NMDA induced dilation of cortical vessel in slices from sham animals, while provoking a constriction of vessels in slices obtained from jmTBI 1 dpi mice. Application of NMDA triggered a greater vasodilation in slices from jmTBI 3dpi as compared to sham. **C.** Quantification of the constriction to U46619 presented as percentage changes as compared to baseline (4–13 animals per group, number of vessels $n = 19$ sham, $n = 5$ jmTBI 1 dpi, $n = 7$ jmTBI 3 dpi, $n = 11$ jmTBI 7 dpi), * $p < .05$, ** $p < .01$, two-way ANOVA, Tukey's multiple comparison test, **D.** Quantification of the vasodilation to NMDA presented as percentage changes as compared to baseline (3–4 animals per group, number of vessels $n = 4$ sham, $n = 4$ jmTBI 1 dpi, $n = 6$ jmTBI 3 dpi) * $p < .05$, ANOVA; scale bar *10 μm.*

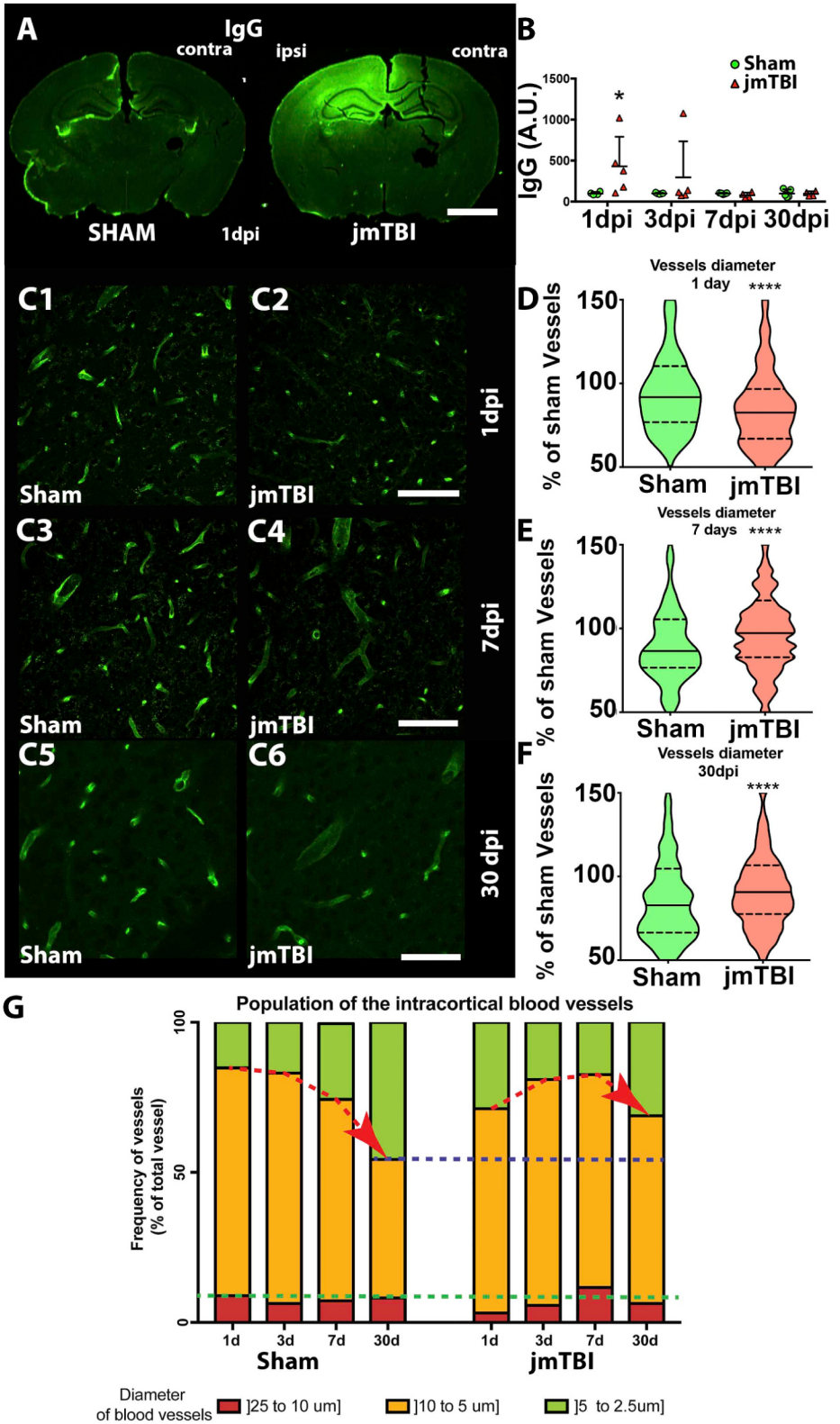


**Fig. 4.** Lingering cerebrovascular histological modifications after jmTBI.
**A.** IgG extravasation at the side of impact in jmTBI mice at 1 dpi; *scale bar 1.5 mm.* **B.** IgG extravasation quantification showed a significant decrease (*$p < 0{,}05$, t-test.; n = 4–5 animals per group). **C.** Intracortical vessels displayed reduced diameter at 1 dpi (C1 sham vs C2 jmTBI) and larger diameters at 7 dpi (C3 sham vs C4 jmTBI) and 30 dpi (C4 sham vs C5 jmTBI); *scale bar 40 μm.* **D.** Quantification plots indicated as percentage to sham. We used, 3–5 animals per group and time-point, 1dpi ****$p < .0001$, $n = 191$ sham vessels, $n = 225$ jmTBI 1 dpi vessels. **E.** Quantification of vessels diameter at 7 dpi ****$p < .0001$, Mann Whitney test $n = 292$ sham vessels vs $n = 325$ jmTBI 7 dpi vessels. **F.** Quantification of vessels diameter at 30 dpi ****$p < .0001$, Mann Whitney test $n = 786$ sham vessels vs $n = 826$ jmTBI 30 dpi vessels. **G.** Distribution of cortical vessel diameters (lectin staining) at 1,3,7 and 30 days after jmTBI and sham. The number of blood vessels was quantified for: 1) vessels with a diameter between 25 μm to 10 μm; 2) vessels with a diameter between 10 μm and equal to 5 μm; 3) blood vessels with a diameter < 5 μm). At 30 dpi, cortical blood vessel populations differ between jmTBI and sham with a reduced number of microvessels <5 μm of diameter.

*4.1. Does cerebrovascular dysfunction constitute an early contributor or a biomarker of long-term neurological sequel in mTBI?*

In our study we asked whether early cerebrovascular damage partake to jmTBI pathophysiology. Accumulating evidence supports a key role of cerebrovascular damage or dysfunction in CNS diseases. Clinical and experimental evidence exists for epilepsy (Bar-Klein et al., 2017; Klement et al., 2018; Librizzi et al., 2018; Marchi and Lerner-Natoli, 2013), neurodegeneration (Boussadia et al., 2016; Giannoni et al., 2016; Giannoni et al., 2020; Sweeney et al., 2019) and moderate or severe forms of pediatric TBI (Jullienne et al., 2014; Pop and Badaut, 2011; Pop et al., 2013) where decrease of cerebral blood flow (CBF) and blood-brain barrier (BBB) permeability can accelerate the development of disease states. BBB alteration is associated with abnormal neuronal activity (Seiffert et al., 2004) by a mechanism of lost brain homeostasis. Our findings are consistent with cerebrovascular determinant(s) of

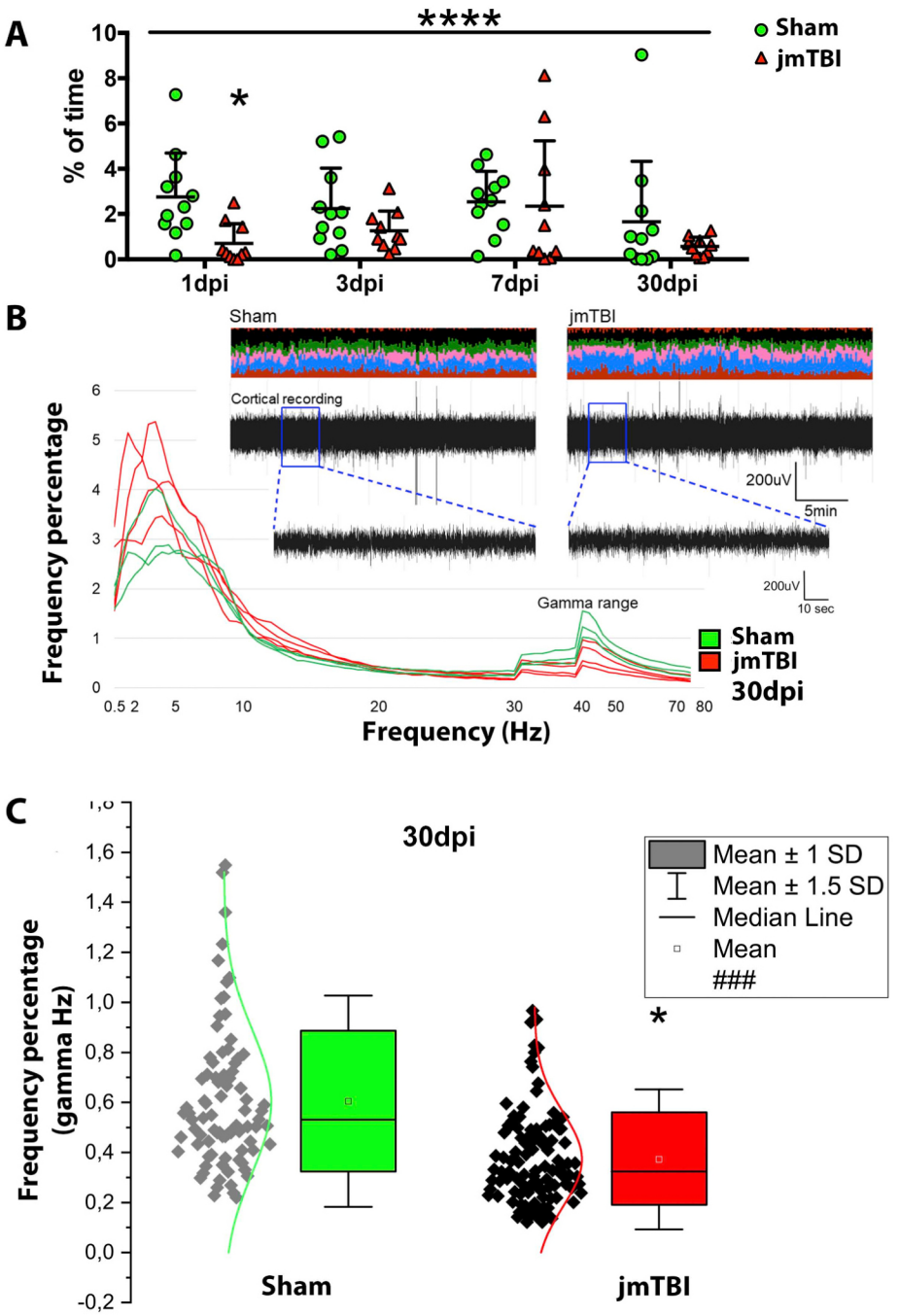


**Fig. 5.** Signs of long-term neurological modifications post jmTBI.
**A.** jmTBI animals spent less time in the center of the open field (two-way ANOVA, *p < .05, Sidak's multiple comparison test, group effect over time *** $p < .001$) n = 11 shams, n = 10 jmTBI at each time-point **B.** Examples of EEG recordings for sham and jmTBI mice at 2 different time scales, and colour-coded on-line frequency distribution as obtained using Neuroscore (0.5–4 Hz red, 4–8 Hz blue, 8–12 Hz pink, 12–30 Hz green and 30–80 Hz black). Mouse specific frequency spectrograms (0.5–80 Hz) from impacted (n = 4; red) and sham mice (n = 3; r green) acquired at 30 dpi. The recording site topographically corresponded to the impacted cortical region. All impacted mice display a decrease of percentage gamma waves as compared to sham. **C)** Box plot indicating percentage of gamma waves in jmTBI and sham conditions. Each data point corresponds to one specific EEG extract obtained from each recording (see methods). (For interpretation of the references to colour in this figure legend, the reader is referred to the web version of this article.)

brain diseases with a relevance to pediatric mTBI, as also previously postulated for severe forms of TBI (Launey et al., 2019; Tomkins et al., 2011; Tomkins et al., 2007).

In our study cerebrovascular oxygenation level returns to physiological values at 3 dpi. Interestingly, decrease of CBF was reported in closed head injury and a controlled cortical impact model in adult mice and rats (Buckley et al., 2015; Long et al., 2015; Villapol et al., 2014) . Modified vasoreactivity, as we here observed *ex vivo* (Fig. 3), could represent one contributor to the oxygenation drop observed *in vivo* (Fig. 2). (Long et al., 2015).

Functional alterations of pial blood vessels were previously reported shortly after moderate or severe TBI in newborn piglets, including increased vasoconstriction after NMDA application on pial blood vessels (Armstead et al., 2011a; Armstead et al., 2011b; Armstead and Kreipke, 2011; Armstead and Raghupathi, 2011). Our data showed that cortical arterioles exhibited dysfunction of vascular contractility after NMDA application at 1 and 3 dpi (Fig. 3). We here acknowledge that we were not able to identify the molecular and cellular mechanisms promoting vascular modifications. For instance, we here report no changes of the thromboxane receptor expression and no changes in the total level of contractile smooth muscle actin (see Supplementary Fig. 3).

A transient loss of cortical intraparenchymal blood vessels was reported after moderate and severe TBI at 1 dpi (Obenaus et al., 2017; Salehi et al., 2017), followed by an abnormal recovery at 2 weeks (Park et al., 2009). In our study we found early modifications of vessels diameter distribution after jmTBI lasting up to 30 dpi (Fig. 4). Early decreased of blood vessel diameter parallels increase BBB permeability to IgG (Fig. 4) as we previously described for this model in the corpus callosum (Rodriguez-Grande et al., 2018). Further exploration is needed to characterize the morphological and functional changes occurring at the vascular mural cells level (Klement et al., 2019). Increase blood-vessel diameter at 30dpi hint to vascular remodeling occurring in

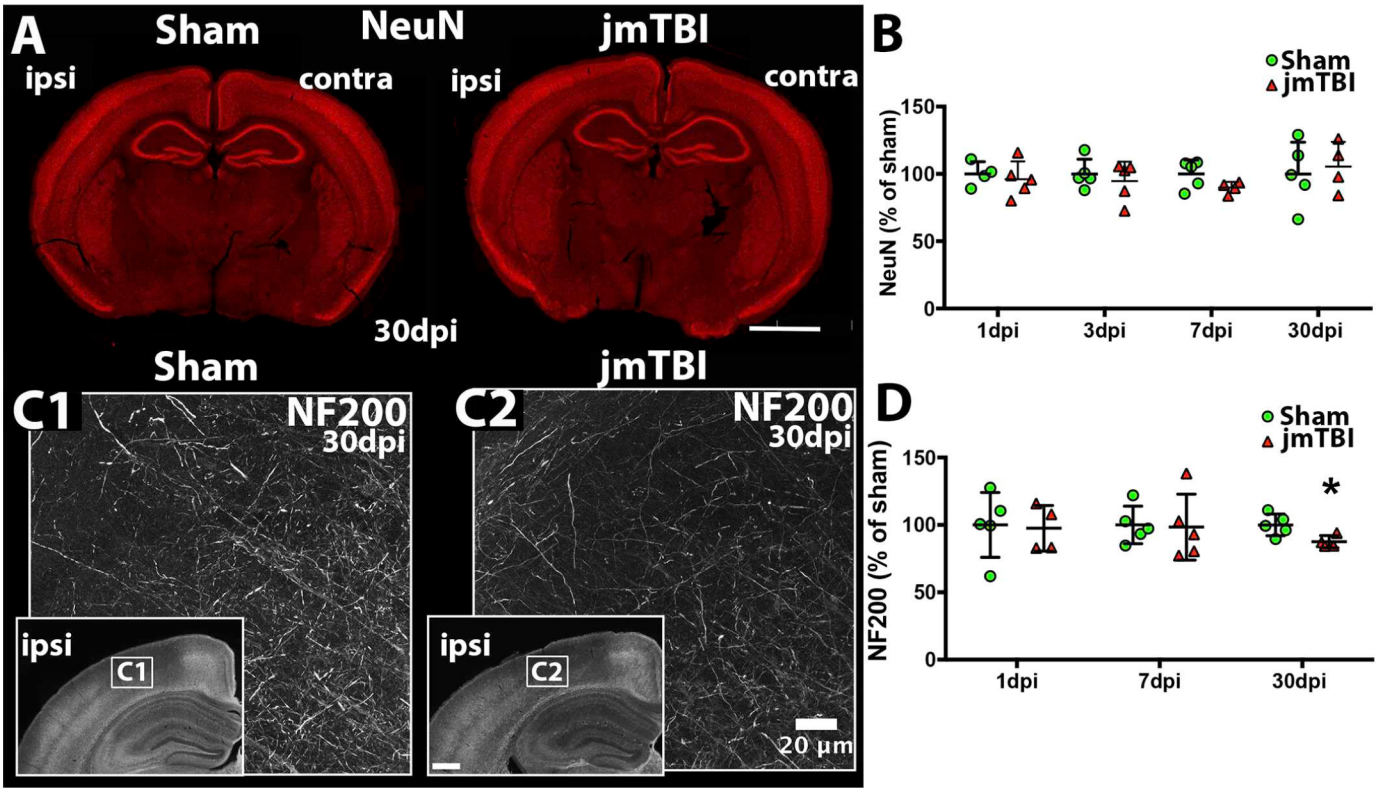


**Fig. 6.** Signs of axonal damage long-term after jmTBI.
**A.** NeuN immunolabelling in Sham and jmTBI showed no difference **B.** Quantification of NeuN immunofluorescence in the ipsilateral cortex over time (data presented as percentage of sham, $p > .05$) $n = 4–5$ animals per group; *scale bar 1.5 mm*. **C.** jmTBI 30 dpi mice (C2) displayed a decrease NF200 immunofluorescence in the ipsilateral cortex as compared to sham (C1); scale bar 20 µm. Picture insert – low magnification acquisitions in the ipsilateral hemisphere, scale bar 500 µm. **D.** Quantification of NF200 staining in the ipsilateral cortex showed significant decrease only at 30 dpi, suggesting delayed axonal damage ($*p < .05$, t-test, $n = 4–5$ animals per group).

the developing brain as a long-term consequence of jmTBI, as previously reported for moderate and severe TBI (Jullienne et al., 2014; Pop et al., 2013). Long-term pathological sequels are also neuronal modification with decreased NF200 staining in the somatosensorial cortex (Fig. 5), although without neuronal loss (Clément et al., 2020). Understanding the molecular and cellular events underlying these changes will require further explorations.

### *4.2. Clinical and experimental clues supporting a neurovascular mechanism of TBI sequel*

Clinical studies have reported reductions of CBF, impaired autoregulation and cerebrovascular reactivity in pediatric TBI (Adelson et al., 2011; Ichkova et al., 2017; Vavilala et al., 2004; Vavilala et al., 2008). The cerebrovascular dysfunction may associate with poor behavioral outcomes, and our data support this hypothesis. Transient neurovascular changes observed after a single jmTBI are coherent with previous clinical reports. Furthermore, patients with persistent post-concussive symptoms demonstrated a reduction of CBF (Bartnik-Olson et al., 2014) up to 30 days post injury (Maugans et al., 2012), suggesting a longer time for vascular remodeling. It is important to note that decreased CBF during high glucose demand creates an energy metabolic mismatch. It is plausible to predict that, under these conditions, a second mTBI would promote an accumulation of brain damage (Fujita et al., 2012; Kamins and Giza, 2016; Miyauchi et al., 2013). Vascular dysfunction could represent an interesting biomarker to assess recovery after mTBI.

Importantly, we observed behavioral deficits as early as 1 dpi, reappearing at 30 dpi (Fig. 5A). The latter results are consistent with long-term behavioral dysfunction (e.g., anxiety), as previously shown in this model (Rodriguez-Grande et al., 2018). Our initial EEG monitoring did not indicate spontaneous seizure activity at 30 days after jmTBI. Nevertheless, the subtle electrocorticographic modifications reported long-term post jmTBI align with the existence of behavioral modifications, as reported here and in previous work for this experimental model (Rodriguez-Grande et al., 2018). Modifications of EEG gamma waves were previously suggested as a sign of impaired neurological functions or neuronal damage (Iaccarino et al., 2016; Kitchigina, 2018; Mably and Colgin, 2018). We speculated that the neurophysiological outcomes here described could be linked to the modifications of cortical neuronal fibers (Fig. 6) and blood vessels (Fig. 4) at 30dpi. Further investigations are required to directly link neurophysiology to neurovascular modifications over time and within the same animal.

### *4.3. Study limitations and conclusions*

Our study has several limitations: **i)** only males were use used. However, females can show worse long-term negative outcomes as compared to males (McEvoy et al., 2019). Moreover, females are more likely to sustain a concussion than males in sport (Bretzin et al., 2018; Covassin et al., 2003). Further studies need to investigate our findings in females. There is evidence for different cerebrovascular recovery (Jullienne et al., 2018b) and neuroinflammatory modifications between males and females after trauma (Jullienne et al., 2018b; Villapol et al., 2017); **ii)** anesthesia, representing a possible confounding factor to pathophysiology and post-traumatic outcomes (Petraglia et al., 2014b; Pham et al., 2019). Studies have reported that repeated isoflurane exposure can modify brain structure and neurological outcomes (Bajwa et al., 2019); **iii)** independent cohorts (Fig. 1A), therefore the direct association between early cerebrovascular dysfunction and long-term

neurological sequel was not examined.

Taken together, our results support the hypothesis that an early cerebrovascular pathology may contribute to long-term and negative neurological sequelae post jmTBI. Further research effort is required to understand the cellular and molecular players involved in the neurovascular pathological process unfolding overtime in this disease setting.

## Sources of funding

This study was supported by grants Eranet neuron CNS-aflame & TRAIN, BIS-Idex, TRAIL-Labex ANR (JB), Foundation des gueules cassées (AI, JB), Idex funding (AO, JB), ANR-Epicyte (NM), Neu-Vasc ANR/Eranet (JB, NM) and grant RETP from the Fondation Leducq.

## Authors' contributions

AI contributed to the experimental design, generated and analyzed histology, Western blot and vascular reactivity data and co-wrote the manuscript; BRG and MLF generated behavior data, JA contributed to generating histology data; EZ and AS performed EEG surgeries, recordings and analysis. PS performed photoacoustic monitoring and data analysis; AO contributed to the experimental design, generated and analyzed T2WI data and took part in writing of the manuscript; JB and NM planned the experimental design. NM analyzed photoacoustic and EEG results and co-wrote the whole manuscript with JB.

## Declaration of Competing Interest

None.

## Acknowledgements

We would like to thank the contribution of Dr. Sandrine Bertrand, Gilles Courtand, Anthony Harster, Frederic deBock, IPAM platform, Montpellier, Phycell platform, INCIA, Bordeaux to the work included in this manuscript.

## References

Adelson, P.D., et al., 2011. Cerebrovascular response in children following severe traumatic brain injury. Childs Nerv. Syst. 27, 1465–1476.

Anderson, V., et al., 2012. 10 years outcome from childhood traumatic brain injury. Int. J. Dev. Neurosci. 30, 217–224.

Armstead, W.M., Kreipke, C.W., 2011. Endothelin-1 is upregulated after traumatic brain injury: a cross-species, cross-model analysis. Neurol. Res. 33, 133–136.

Armstead, W.M., Raghupathi, R., 2011. Endothelin and the neurovascular unit in pediatric traumatic brain injury. Neurol. Res. 33, 127–132.

Armstead, W.M., et al., 2011a. Glucagon protects against impaired NMDA-mediated cerebrovasodilation and cerebral autoregulation during hypotension after brain injury by activating cAMP protein kinase a and inhibiting upregulation of tPA. J. Neurotrauma 28, 451–457.

Armstead, W.M., et al., 2011b. tPA contributes to impaired NMDA cerebrovasodilation after traumatic brain injury through activation of JNK MAPK. Neurol. Res. 33, 726–733.

Babikian, T., et al., 2015. Chronic aspects of pediatric traumatic brain injury: review of the literature. J. Neurotrauma 32, 1849–1860.

Badaut, J., et al., 2011. Brain water mobility decreases after astrocytic aquaporin-4 inhibition using RNA interference. J. Cereb. Blood Flow Metab. 31, 819–831.

Bajwa, N.M., et al., 2019. Repeated isoflurane in adult male mice leads to acute and persistent motor decrements with long-term modifications in corpus callosum microstructural integrity. J. Neurosci. Res. 97, 332–345.

Barkhoudarian, G., et al., 2016. The molecular pathophysiology of concussive brain injury - an update. Phys. Med. Rehabil. Clin. N. Am. 27, 373–393.

Bar-Klein, G., et al., 2017. Imaging blood-brain barrier dysfunction as a biomarker for epileptogenesis. Brain 140, 1692–1705.

Bartnik-Olson, B.L., et al., 2014. Impaired neurovascular unit function contributes to persistent symptoms after concussion: a pilot study. J. Neurotrauma 31, 1497–1506.

Blanco, V.M., et al., 2008. Tone-dependent vascular responses to astrocyte-derived signals. Am. J. Physiol. Heart Circ. Physiol. 294, H2855–H2863.

Boussadia, B., et al., 2016. Lack of CAR impacts neuronal function and cerebrovascular integrity in vivo. Exp. Neurol. 283, 39–48.

Boussadia, B., et al., 2018. Pregnane X receptor deletion modifies recognition memory and electroencephalographic activity. Neuroscience 370, 130–138.

Bretzin, A.C., et al., 2018. Sex differences in the clinical incidence of concussions, missed school days, and time loss in high school student-athletes: part 1. Am. J. Sports Med. 46, 2263–2269.

Buckley, E.M., et al., 2015. Decreased microvascular cerebral blood flow assessed by diffuse correlation spectroscopy after repetitive concussions in mice. J. Cereb. Blood Flow Metab. 35, 1995–2000.

Clément, T., Lee, J.B., Ichkova, A., Rodriguez-Grande, B., Fournier, M.L., Aussudre, J., Ogier, M., Haddad, E., Canini, F., Koehl, M., Abrous, D.N., Obenaus, A., Glia, Badaut J., 2020 Mar. Juvenile mild traumatic brain injury elicits distinct spatiotemporal astrocyte responses. 68 (3). https://doi.org/10.1002/glia.23736. Epub 2019 Oct 31. PMID: 31670865.

Covassin, T., et al., 2003. Sex differences and the incidence of concussions among collegiate athletes. J. Athl. Train. 38, 238–244.

Dean, P.J., Sterr, A., 2013. Long-term effects of mild traumatic brain injury on cognitive performance. Front. Hum. Neurosci. 7, 30.

Fujita, M., et al., 2012. Intensity- and interval-specific repetitive traumatic brain injury can evoke both axonal and microvascular damage. J. Neurotrauma 29, 2172–2180.

Giannoni, P., et al., 2016. Cerebrovascular pathology during the progression of experimental Alzheimer's disease. Neurobiol. Dis. 88, 107–117.

Giannoni, P., et al., 2018. The pericyte-glia interface at the blood-brain barrier. Clin. Sci. (Lond.) 132, 361–374.

Giannoni, P., et al., 2020. Peripheral routes to neurodegeneration: passing through the blood-brain barrier. Front. Aging Neurosci. 12, 3.

Girard, B., et al., 2019. The mGlu7 receptor provides protective effects against epileptogenesis and epileptic seizures. Neurobiol. Dis. 129, 13–28.

Iaccarino, H.F., et al., 2016. Gamma frequency entrainment attenuates amyloid load and modifies microglia. Nature 540, 230–235.

Ichkova, A., et al., 2017 Dec. Vascular impairment as a pathological mechanism underlying long-lasting cognitive dysfunction after pediatric traumatic brain injury. Neurochem. Int. 111, 93–102. https://doi.org/10.1016/j.neuint.2017.03.022. Epub 2017 Apr 1.PMID: 28377126.

Jullienne, A., et al., 2014 Oct. Juvenile traumatic brain injury induces long-term perivascular matrix changes alongside amyloid-beta accumulation. J. Cereb. Blood Flow Metab. 34 (11), 1637–1645. https://doi.org/10.1038/jcbfm.2014.124. Epub 2014 Jul 23.PMID: 25052558.

Jullienne, A., et al., 2018a. Modulating the water channel AQP4 alters miRNA expression, astrocyte connectivity and water diffusion in the rodent brain. Sci. Rep. 8, 4186.

Jullienne, A., et al., 2018b. Male and female mice exhibit divergent responses of the cortical vasculature to traumatic brain injury. J. Neurotrauma 35, 1646–1658.

Kamins, J., Giza, C.C., 2016. Concussion-mild traumatic brain injury: recoverable injury with potential for serious Sequelae. Neurosurg. Clin. N. Am. 27, 441–452.

Kitchigina, V.F., 2018. Alterations of coherent Theta and gamma network oscillations as an early biomarker of temporal lobe epilepsy and Alzheimer's disease. Front. Integr. Neurosci. 12, 36.

Klement, W., et al., 2018. Seizure progression and inflammatory mediators promote pericytosis and pericyte-microglia clustering at the cerebrovasculature. Neurobiol. Dis. 113, 70–81.

Klement, W., et al., 2019. A pericyte-glia scarring develops at the leaky capillaries in the hippocampus during seizure activity. Epilepsia 60, 1399–1411.

Launey, Y., et al., 2019 Nov 11. Spatial and temporal pattern of ischemia and abnormal vascular function following traumatic brain injury. JAMA Neurol. 77 (3), 339–349. https://doi.org/10.1001/jamaneurol.2019.3854.

Librizzi, L., et al., 2018. Cerebrovascular heterogeneity and neuronal excitability. Neurosci. Lett. 667, 75–83.

Long, J.A., et al., 2015. The effects of perturbed cerebral blood flow and cerebrovascular reactivity on structural MRI and behavioral readouts in mild traumatic brain injury. J. Cereb. Blood Flow Metab. 35, 1852–1861.

Lumba-Brown, A., et al., 2018. Diagnosis and management of mild traumatic brain injury in children: a systematic review. JAMA Pediatr. 172, e182847.

Mably, A.J., Colgin, L.L., 2018. Gamma oscillations in cognitive disorders. Curr. Opin. Neurobiol. 52, 182–187.

Marchi, N., Lerner-Natoli, M., 2013. Cerebrovascular remodeling and epilepsy. Neuroscientist 19, 304–312.

Maugans, T.A., et al., 2012. Pediatric sports-related concussion produces cerebral blood flow alterations. Pediatrics 129, 28–37.

McEvoy, H., et al., 2019 Dec 22. Clinical features and sex differences in pediatric post-traumatic headache: a retrospective chart review at a Boston area concussion clinic. Cephalalgia. https://doi.org/10.1177/0333102419896754. 333102419896754.

Miyauchi, T., et al., 2013. Therapeutic targeting of the axonal and microvascular change associated with repetitive mild traumatic brain injury. J. Neurotrauma 30, 1664–1671.

Montagne, A., et al., 2017. Alzheimer's disease: a matter of blood-brain barrier dysfunction? J. Exp. Med. 214, 3151–3169.

Obenaus, A., et al., 2017. Traumatic brain injury results in acute rarefication of the vascular network. Sci. Rep. 7, 239.

Park, E., et al., 2009. An analysis of regional microvascular loss and recovery following two grades of fluid percussion trauma: a role for hypoxia-inducible factors in traumatic brain injury. J. Cereb. Blood Flow Metab. 29, 575–584.

Petraglia, A.L., et al., 2014a. Models of mild traumatic brain injury: translation of physiological and anatomic injury. Neurosurgery 75 (Suppl. 4), S34–S49.

Petraglia, A.L., et al., 2014b. The spectrum of neurobehavioral sequelae after repetitive mild traumatic brain injury: a novel mouse model of chronic traumatic encephalopathy. J. Neurotrauma 31, 1211–1224.

Pham, L., et al., 2019. Mild closed-head injury in conscious rats causes transient

neurobehavioral and glial disturbances: a novel experimental model of concussion. J. Neurotrauma 36, 2260–2271.
Philip, S., et al., 2009. Cerebrovascular pathophysiology in pediatric traumatic brain injury. J. Trauma 67, S128–S134.
Pop, V., Badaut, J., 2011. A neurovascular perspective for long-term changes after brain trauma. Transl. Stroke Res. 2, 533–545.
Pop, V., et al., 2013. Early brain injury alters the blood-brain barrier phenotype in parallel with beta-amyloid and cognitive changes in adulthood. J. Cereb. Blood Flow Metab. 33, 205–214.
Rancillac, A., et al., 2006. Glutamatergic control of microvascular tone by distinct GABA neurons in the cerebellum. J. Neurosci. 26, 6997–7006.
Rodriguez-Grande, B., et al., 2018 Aug. Gliovascular changes precede white matter damage and long-term disorders in juvenile mild closed head injury. Glia 66 (8), 1663–1677. https://doi.org/10.1002/glia.23336. Epub 2018 Apr 17.PMID: 29665077.
Salehi, A., et al., 2017. Response of the cerebral vasculature following traumatic brain injury. J. Cereb. Blood Flow Metab. 37, 2320–2339.
Seiffert, E., et al., 2004. Lasting blood-brain barrier disruption induces epileptic focus in the rat somatosensory cortex. J. Neurosci. 24, 7829–7836.
Sweeney, M.D., et al., 2019. Blood-brain barrier: from physiology to disease and Back. Physiol. Rev. 99, 21–78.
Tomkins, O., et al., 2007. Blood-brain barrier disruption results in delayed functional and structural alterations in the rat neocortex. Neurobiol. Dis. 25, 367–377.
Tomkins, O., et al., 2011. Blood-brain barrier breakdown following traumatic brain injury: a possible role in posttraumatic epilepsy. Cardiovasc. Psychiatry Neurol. 2011, 765923.
Vavilala, M.S., et al., 2004. Cerebral autoregulation in pediatric traumatic brain injury. Pediatr. Crit. Care Med. 5, 257–263.
Vavilala, M.S., et al., 2008. Hemispheric differences in cerebral autoregulation in children with moderate and severe traumatic brain injury. Neurocrit. Care. 9, 45–54.
Villapol, S., et al., 2014. Temporal dynamics of cerebral blood flow, cortical damage, apoptosis, astrocyte-vasculature interaction and astrogliosis in the pericontusional region after traumatic brain injury. Front. Neurol. 5, 82.
Villapol, S., et al., 2017. Sexual dimorphism in the inflammatory response to traumatic brain injury. Glia. 65, 1423–1438.
Zonta, M., et al., 2003. Neuron-to-astrocyte signaling is central to the dynamic control of brain microcirculation. Nat. Neurosci. 6, 43–50.
Zub, E., et al., 2019. The GR-ANXA1 pathway is a pathological player and a candidate target in epilepsy. FASEB J. 33, 13998–14009.